




Engineering defect concentrations of multiwalled carbon nanotubes by microwave irradiation for tunable electromagnetic absorption properties

Yujuan Song^{1,2}, Huawei Rong^{1,2}, Yixing Li^{1,2}, Weiwei Liu², and Xuefeng Zhang^{1,2,*} 

¹Key Laboratory for Anisotropy and Texture of Materials (MOE), School of Materials Science and Engineering, Northeastern University, Shenyang 110819, People's Republic of China

²Institute of Advanced Magnetic Materials, Hangzhou Dianzi University, Hangzhou 310012, People's Republic of China

Received: 17 March 2020

Accepted: 18 June 2020

Published online:
25 June 2020

© Springer Science+Business
Media, LLC, part of Springer
Nature 2020

ABSTRACT

Incorporating the dielectric polarization effect induced by atomic-scale structural defects is an effective strategy to improve the electromagnetic absorption performances of materials. Herein, the defect concentration of multiwalled carbon nanotubes (MWCNTs) could be tuned by irradiation time under the 2.45 GHz microwave, depending on the localized “heat” effect. The defect density of the mostly optimized MWCNTs treated by irradiation for 4 min reached a maximum, presenting the defect distance (L_D) of 10.83 nm and the concentration (n_D) of $2.76 \times 10^{11} \text{ cm}^{-2}$, achieving the maximum effective absorption bandwidth of 5 GHz, which is higher than original-carbon nanotubes (CNTs) (3.9 GHz). Different from the previous integration of CNTs and heterogeneous magnetic metals, the present work demonstrates a simple microwave irradiation approach for tailoring the electromagnetic absorption properties of MWCNTs by engineering the defect concentration, and this could be extended to variable carbon-related materials and diverse applications.

Introduction

With the rapid development of electronic information technology, various types of digital and high-frequency electronic and electrical equipment radiate a large number of electromagnetic waves of different wavelengths into space, thus causing electromagnetic interference. Therefore, the research of microwave

absorbers has attracted wide attention to improve the anti-interference ability of electronic devices and solve the pollution problem of electromagnetic wave [1–6].

Since its discovery in 1991 [7], the unique structural characteristics, conductivity and mechanical properties of CNTs indicate that it has a broad development prospect in the field of microwave absorption materials [8, 9]. Generally speaking, CNTs is a typical

Address correspondence to E-mail: zhangxf@atm.neu.edu.cn

dielectric loss material, and the microwave loss capacity is closely related to the polarization of internal dipoles. In addition, tubular structure gives it a high specific surface area, so multiple scattering of electromagnetic waves can occur inside [10]. In recent years, some excellent CNTs microwave absorbing materials mainly rely on complex permittivity ($\epsilon_r = \epsilon' + i\epsilon''$), complex permeability ($\mu_r = \mu' + i\mu''$) and their impedance matching, usually with the aid of CNTs/ferromagnetic metal composites or CNTs/polymer composites [11–15]. However, the synthesis methods of such complex composite materials are generally complicated, and the mechanism of interaction between them is still under discussion [16, 17]. Recently, studies have shown that CNTs containing defects exert high real permittivity and can be utilized as promising dielectric loss materials with electromagnetic absorption [18]. Therefore, Li and Chen et al. used this property of defective CNTs to introduce them into carbonyl iron-based composite materials, and improved their microwave absorption properties by doping effect and electromagnetic matching [19]. Wei and Yin et al. prepared CNTs with different defect concentrations on porous $\text{Sc}_2\text{Si}_2\text{O}_7$ matrix by using chemical vapor deposition method and adjusting reaction time. The resulting defects were dipole polarized, thus affecting the band gap of carbon nanotubes and providing new thinking for the development of electromagnetic absorbing materials [20]. Wu et al. [21] prepared cerium oxide nanoparticles decorated MWCNTs composites with oxygen-rich vacancy defects by hydrothermal method, in which the three-dimensional conductive grid and oxygen vacancy are beneficial to improving the electromagnetic absorption performance. Conventional CNTs microwave absorbing materials are mostly composed of magnetic metal and dielectric carbon components, and the complex components constructed make it difficult to understand the interaction between electromagnetic waves and substances. Considering that the introduction of defects into MWCNTs causes changes in microwave absorption characteristics, here we construct pure defective MWCNTs.

In this study, we regulated the microwave absorption properties of MWCNTs by modulating the degree of defects. The result reveals that a simple treatment with microwave irradiation can effectively adjust the defect concentration of MWCNTs and reaches the maximum defect degree in 4 min, which

leading to the obvious change of microwave absorption performance.

Experiments

Preparation

MWCNTs were purchased from Nanjing Pioneer Nano Material Technology Co., Ltd., with average length of 10–30 μm , dimensions of < 8 nm and purity of $> 98\%$. 2 g of MWCNTs were dispersed in 100 ml of 6.82 mol/L HNO_3 , and refluxed in a three-necked flask at 140 $^\circ\text{C}$ for 9 h. After cooling down to room temperature, the solution was filtered through a PTFE membrane with a pore size of 0.22 μm and rinse with deionized water until the pH of the filtrate was around 7. The produced product was dried in an oven at 60 $^\circ\text{C}$ for 12 h. Finally, under the protective atmosphere of argon, 0.5 g of MWCNTs were treated with microwave irradiation for 0 min, 2 min, 4 min, 6 min, 8 min and 10 min, respectively, named MI0-CNTs, MI2-CNTs, MI4-CNTs, MI6-CNTs, MI8-CNTs and MI10-CNTs. A household microwave oven with a frequency of 2.45 GHz was utilized for microwave irradiation.

Characterization

Microstructure characterizations: A Raman microscope (model R-XploRA Plus, Horiba, Kyoto) was used to perform Raman spectroscopy analysis at a laser excitation wavelength of 532 nm, with a power attenuation of 1 mW. X-ray diffraction (XRD) was recorded by a Rigaku SmartLab X-ray diffractometer with CuK_α ($\lambda = 0.154$ nm) radiation at a voltage of 30 kV and a current of 30 mA at a scan step of 0.02° .

Electromagnetic measurements: The Vector Network Analyzer (Keysight N5222A) was calibrated via a 2 port short-open-load-thru (SOLT) architecture to measure electromagnetic parameters at 2–18 GHz, in which the MI-CNTs was mixed with the paraffin at mass fraction of 20 wt%.

Results and discussion

Microstructure characterizations

Raman spectroscopy has been utilized in this work to examine the changes of defects in irradiated MWCNTs, as shown in Fig. 1a, d. Meanwhile, the Raman spectra of MI6-CNTs and MI10-CNTs have been shown in supplementary Fig. S1 which has been employed to prove the relationship between microwave irradiation time and defect density. For all samples, there are three characteristic peaks, which are the D peak at 1350 cm^{-1} , the G peak at 1596 cm^{-1} ,

and the 2D peak at 2699 cm^{-1} . It is well known that the D-peak of carbon-based materials is derived from the first-order scattering process of sp^2 carbon atoms, representing the first-order scattering of A_{1g} mode, the G-peak is derived from the stretching motion of sp^2 , corresponding to the first-order scattering of E_{2g} mode, and the 2D peak is the second-order mode of the D-peak, derived from the double resonance process involving two phonons with opposite motions [22, 23]. Among them, the increased ratio between the intensities of the D peak and the G peak (I_D/I_G) can be explained in terms of an enhanced density of structural defects degree of sample, which is triggered by

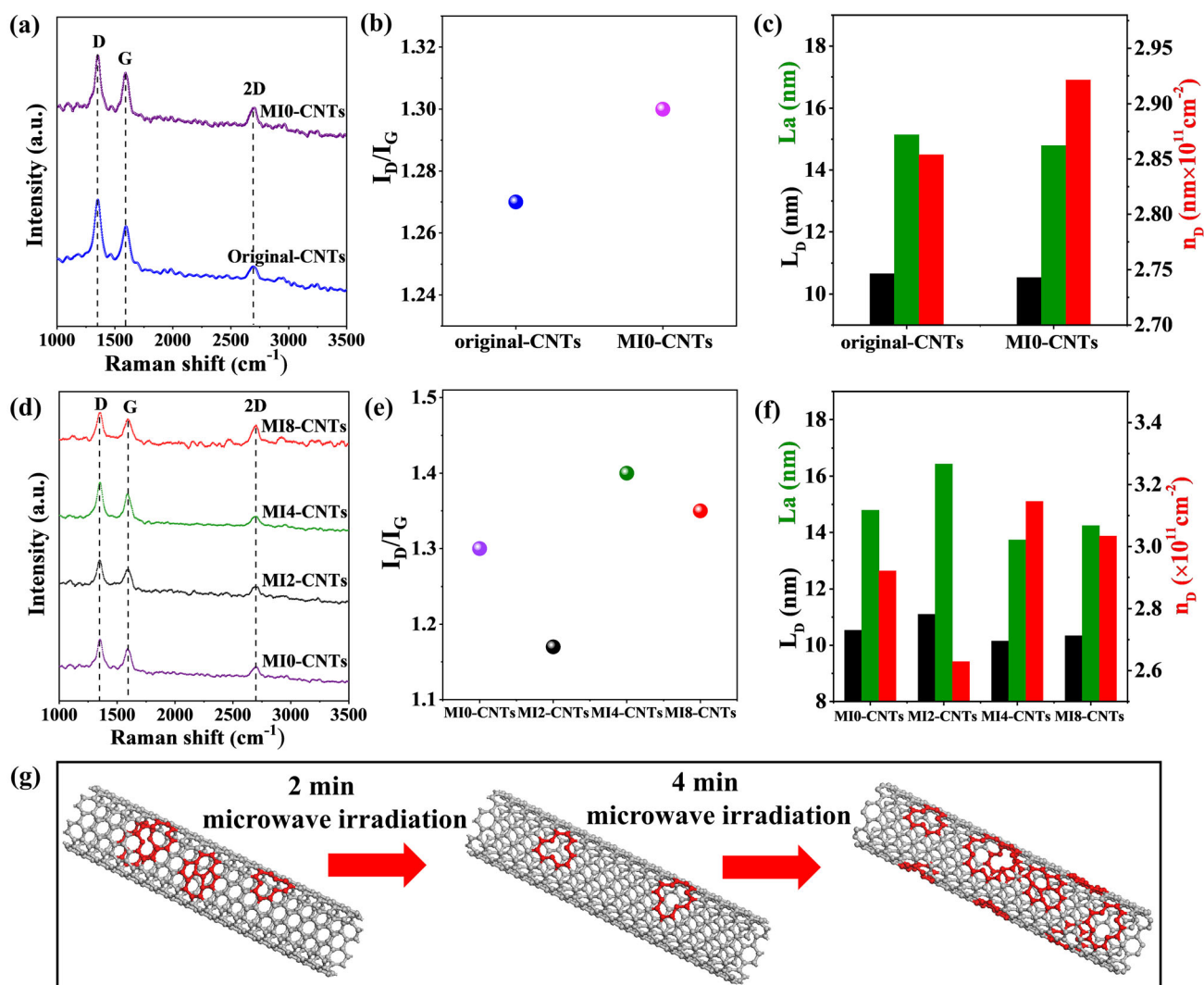


Figure 1 Raman spectra of five kinds of MWCNTs. **a** Raman spectroscopy of D, G and 2D bands of original-CNTs and MI0-CNTs; **b** I_D/I_G for original-CNTs and MI0-CNTs; **c** the crystalline domains L_a , defect distance L_D , and defect sites n_D for original-CNTs and MI0-CNTs; **d** Raman spectroscopy of D, G and 2D

bands of MI0-CNTs, MI2-CNTs, MI4-CNTs and MI8-CNTs; **e** I_D/I_G for MI0-CNTs, MI2-CNTs, MI4-CNTs and MI8-CNTs; **f** the crystalline domains L_a , defect distance L_D , and defect sites n_D for MI0-CNTs, MI2-CNTs, MI4-CNTs and MI8-CNTs; **g** schematic diagram of defect changes during microwave irradiation.

the increasing deviation of the crystalline arrangement from perfect hexagonal planar C network [24]. As shown in Fig. 1b, it has been found that the defect density of MWCNTs treated by HNO₃ etching for 9 h increased compared with the original MWCNTs. Etching MWCNTs with nitric acid can control the defect concentration on the one hand, and dissolve the amorphous carbon and metal catalytic particles such as Fe and Ni remaining in the preparation process of MWCNTs on the other hand, to achieve the purpose of further purification. The oxidation process modified the surface of carbon nanotubes and formed functional groups such as carboxylic (–COOH), carbonyl (–C=O) and hydroxyl (–OH) on the surface, adding more active sites which can respond to subsequent microwave irradiation experiments. With the increase in microwave irradiation time, the defect density in MWCNTs begins to decrease, increases after 2 min, and finally reaches the maximum at 4 min, as displays in Fig. 1e. The decreased defect density in MI2-CNTs indicates that the structural arrangement of MWCNTs has been improved after microwave irradiation process, which is caused by the structural reorganization from defect structures to hexagonal planar C network by absorbing the thermal energy [25]. Figure 1c, f exhibits three parameters related to defects can be calculated based on empirical formulas. The average distance between two defect sites (L_D) can be estimated by Eq. (1) [22, 26–28]:

$$L_D^2(\text{nm}^2) = (1.8 \pm 0.5) \times 10^{-9} \times \lambda^4 \times (I_D/I_G)^{-1} \quad (1)$$

where λ is the incident wavelength of the Raman laser, and I_D and I_G represent the intensities of the D and G peaks, respectively. The obtained defect distances are 10.66 nm, 10.53 nm, 11.10 nm, 10.15 nm and 10.33 nm for original-CNTs, MI0-CNTs, MI2-CNTs, MI4-CNTs and MI8-CNTs, respectively. The n_D represents the concentration of the defect sites, which can be expressed by using Eq. (2) [29], the calculations are $2.85 \times 10^{11} \text{ cm}^{-2}$, $2.92 \times 10^{11} \text{ cm}^{-2}$, $2.62 \times 10^{11} \text{ cm}^{-2}$, $3.15 \times 10^{11} \text{ cm}^{-2}$ and $3.03 \times 10^{11} \text{ cm}^{-2}$, respectively.

$$n_D(\text{cm}^{-2}) = [(1.8 \pm 0.5) \times 10^{22}/\lambda^4] \times (I_D/I_G) \quad (2)$$

The values of the graphite domain size (L_a) which are evaluated based on Eq. (3) [30, 31] are 15.14 nm, 14.79 nm, 16.43 nm, 13.73 nm and 14.24 nm, respectively. Obviously, the decrease in L_a , L_D and the

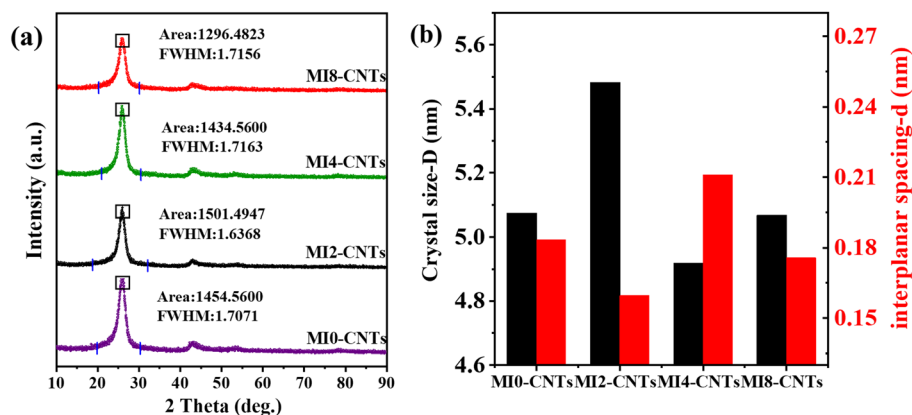
increase in n_D indicate that increasing the microwave irradiation time for more than 2 min will destroy the atomic structure symmetry of the carbon nanotubes, thereby increasing the degree of defects in MI4-CNTs and MI8-CNTs. The defect density reaches a maximum at 4 min during microwave irradiation.

$$L_a(\text{nm}) = (2.4 \times 10^{-10}) \times \lambda^4 \times (I_D/I_G)^{-1} \quad (3)$$

Figure 2a, b represent the X-ray diffraction (XRD) patterns of MI0-CNTs, MI2-CNTs, MI4-CNTs and MI8-CNTs, respectively, illustrating a typical graphite structure. It could be found that the samples irradiated by the microwave possess a structure similar to that of graphite crystal, which indicates that the process does not change the overall structure of the MWCNTs. Figure 2a depicts prominent diffraction peaks appear near 26°, 45° and 54° correspond to the (002), (100) and (004) crystal planes of crystalline graphite, according to graphite in the MDI Jade database (JCPDS No. 26-1076) [32, 33]. The strongest and sharpest diffraction peak of C (002) shows that the structure of the samples was irradiated by microwave without obvious damage.

XRD is a very effective tool for measuring crystal size and interlayer spacing. Measurements of crystal size (D) can be calculated from the peak C (002) which is present at approximately 26° at 2θ and the Scherrer equation [34]. Thus, as shown in Fig. 2b, the crystal sizes (D) are 5.07 nm, 5.48 nm, 4.92 nm and 5.06 nm, respectively. A decrease in grain size in a carbon material causes a broadening of the XRD peak. Therefore, the sample irradiated by microwave for 4 min has the widest FWHM, that is, the lowest crystallinity. However, amounts of it are very little, because the crystal structure of the sample does not change drastically. Crystal refinement leads to an increase in crystal boundary, and the arrangement at the crystal boundary is often distorted and prone to various types of defects, so the defect degree increases, which is consistent with the test results of Raman. An increase in the degree of defects in the MWCNTs causes the diffraction peak to shift slightly toward the low diffraction angle, resulting in the larger interplanar spacing [35]. The interplanar spacings (d) which are calculated based on Bragg equation [36] are 0.18 nm, 0.16 nm, 0.21 nm and 0.17 nm, respectively. It is clear that MI4-CNTs has the largest interplanar spacing, corresponding to the

Figure 2 Phase component characterizations of MIO-CNTs, MI2-CNTs, MI4-CNTs and MI8-CNTs. **a** X-ray diffraction patterns; **b** grain size (D) and interplanar spacing (d).



phenomenon that the diffraction peak was inclined to a low angle caused by the maximum defect density.

Electromagnetic properties

As a heating mode from the inside out, microwave heating can directly act on the reaction sample itself to achieve a macroscopic and uniform thermal effect. In condensed matter physics, microwave heating mechanisms are generally divided into three types: dipolar polarization heating, ion conductor heating and microwave skin effect. For the nitric acid treated MWCNTs, the dipolar polarization heating would contribute the preparation, ascribed to the increasing content of oxygen-containing functional groups such as hydroxyl ($-\text{OH}$) and carboxylic ($-\text{COOH}$) which exhibit polar effect in nature. Under the irradiation of an external microwave energy with a fixed frequency of 2.45 GHz, the corresponding functional groups in the sample would act as the dielectric dipolar and thus oscillate produce violent friction between each other. Consequently, the external microwaves energy causes dielectric polarization and transforms the electromagnetic energy into thermal energy, which displays as a macroscopic thermal effects [37].

To understand the effect of microwave irradiation on the microwave absorption capacity of MWCNTs, we analyzed the electromagnetic properties of MWCNTs at 2–18 GHz using a vector network analyzer. Figure 3a, b show the variation of S_{11} and S_{21} with frequency, where S_{11} and S_{21} represent the reflection coefficient and the transmission coefficient, respectively. Simultaneously, in order to compare quantitatively, the microwave absorption characteristics of these four MWCNTs are calculated using

Eq. (4) [38, 39]. The calculated results are shown in Fig. 3c.

$$A = 1 - |S_{11}|^2 - |S_{21}|^2 \quad (4)$$

From Fig. 3c, it can be seen that the microwave absorption coefficient of the MWCNTs with defects irradiated by microwave is constantly changing with the reaction time. It is clear that the MI4-CNTs with the highest defect concentration has the best microwave absorption coefficient, which is consistent with the result of the defect density in the Raman spectrum. As a result, this phenomenon indicates that MWCNTs with high defect density can produce more polarized positions and can act as electron channels in a low energy state [40], resulting in a higher contribution of defective carbon nanotubes to microwave absorption performance than graphitized carbon nanotubes.

To look into the mechanism of microwave absorption, the variation of complex permittivity and complex permeability with frequency ranging from 2 to 18 GHz was studied, as shown in Fig. 4a–d. Studies on the real part of the complex permittivity of these four MWCNTs find that MI4-CNTs is higher than the other three samples at 2–6 GHz, and multiple resonance peaks occurs at 6–16 GHz. This indicates that high defect content can be used as a polarization center, thus improving the ability to store electromagnetic energy. At the same time, all the ϵ' curves on the whole show a decreasing trend with increasing frequency, indicating that the polarization is delayed under the change of the electric field at a high frequency. In Fig. 4b, the change of the imaginary part of the complex permittivity is more complicated. When the microwave irradiation time is less than 2 min, the imaginary part is completely

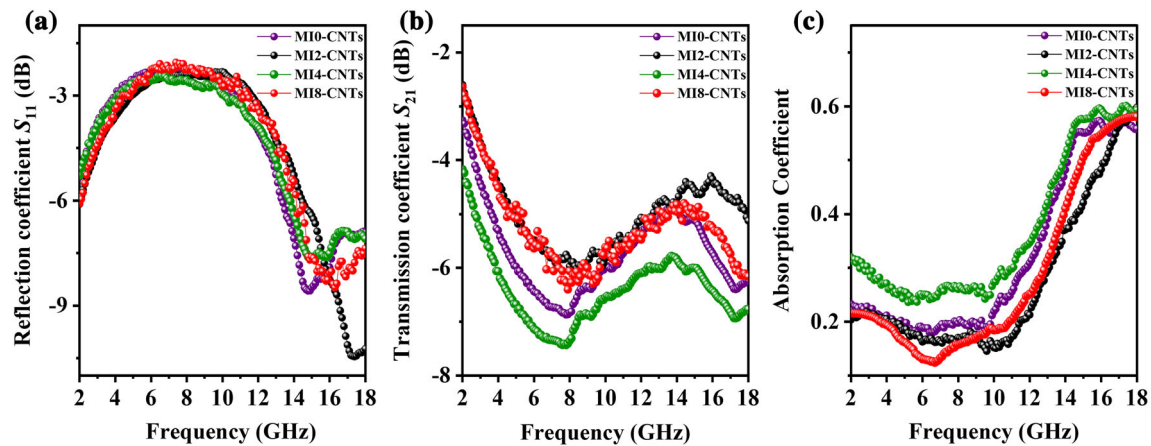
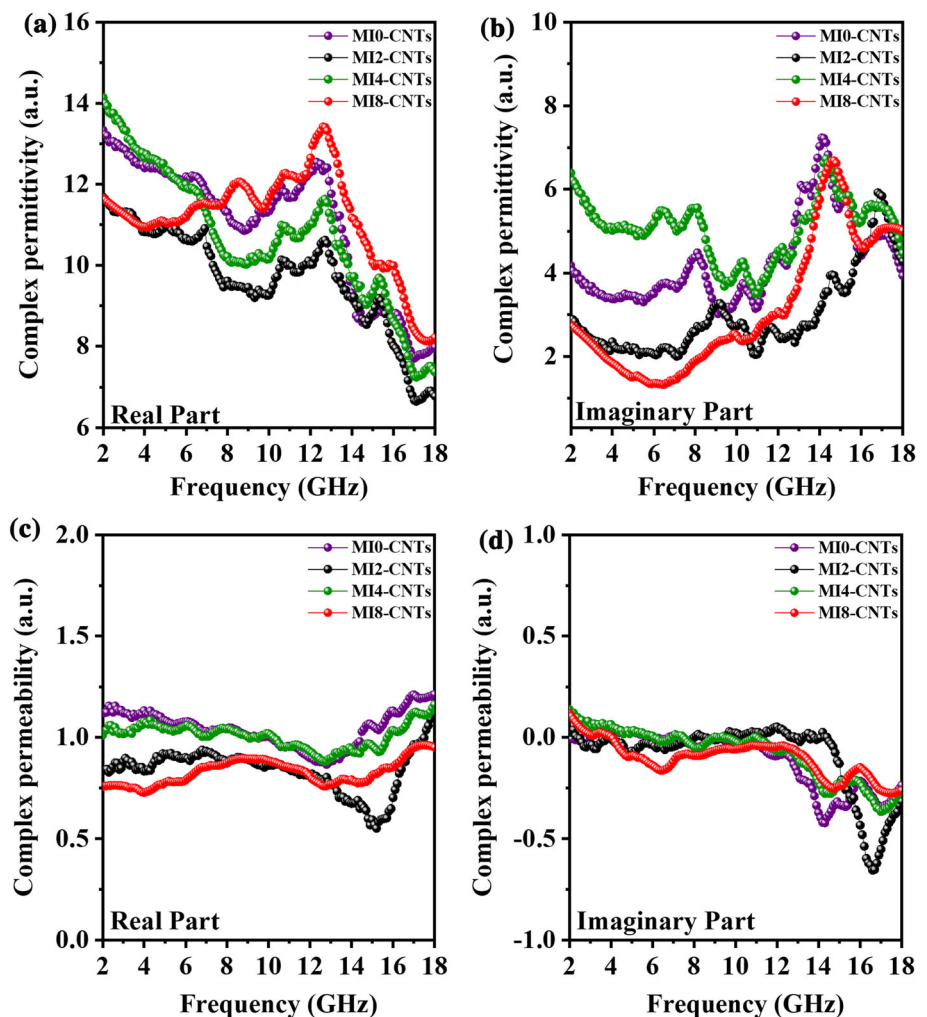


Figure 3 Microwave absorption performances (scattering parameters) of MI0-CNTs, MI2-CNTs, MI4-CNTs and MI8-CNTs. **a** The reflection coefficient (S_{11}) values; **b** the transmission coefficient (S_{21}) values; **c** the absorption coefficient (A) values.

Figure 4 The relatively complex permittivity and permeability of MI0-CNTs, MI2-CNTs, MI4-CNTs and MI8-CNTs. **a** The real part of the relatively complex permittivity; **b** the imaginary part of the relatively complex permittivity; **c** the real part of the relatively complex permeability; **d** the imaginary part of the relatively complex permeability.



reduced. However, when the microwave irradiation time increases to 4 min, the opposite trend is shown. Continue to extend the response time to 8 min, there

is a decline in the results. In particular, the multiple resonance peaks of imaginary part for these four MWCNTs samples could be observed at ~ 8 and

15 GHz, which is associated with the difference of polarization relaxation behavior occurring in the different samples. There are three main sources of polarization relaxation have been exhibited in recent studies: the so-called electronic polarization, ionic polarization, and dipolar polarization [41]. Since the first two polarization behaviors generally occur in the infrared or higher frequency range, the dipolar polarization effect could take domain and thus cause the charge distribution with the increasing defect content at microwave frequency range. Obviously, in the Raman characterization, when the microwave irradiation time are 4 min and 8 min, the defect density is higher, and the dipole polarization effect at this time increases accordingly. The increased defects in the MWCNTs enhance the polarizable effect and increase the dielectric loss, which is mainly because of the MWCNTs is a typical dielectric loss mechanism material. Under the microwave irradiation, electric dipoles are formed on the surface of MWCNTs, which generates the polarization current. In addition, the change of the complex permeability is complex. The real part and imaginary part are about 1 and 0, respectively, as shown in Fig. 4c, d. This phenomenon indicates that the etching process of dilute nitric acid plays a certain role in the pre-treatment process, and the influence of the magnetic catalyst particles is avoided. When testing the electromagnetic performance through the coaxial air line, since the wires of the standard calibration original are particularly sensitive to the errors caused by the calibration and measurement test ports, the test data of the series of samples seem to have certain fluctuations. Therefore, we also provide another new absorbing performance data in supplementary Fig. S2 and Fig. S3, in contrast to the original data.

To further study the microwave absorption capabilities affected by microwave irradiation, the reflection losses (RL) of the MI0-CNTs, MI2-CNTs, MI4-CNTs and MI8-CNTs are estimated by calculation of complex permittivity ($\epsilon_r = \epsilon' + i\epsilon''$) and permeability ($\mu_r = \mu' + i\mu''$) using transmission line theory (Eq. (5) [42]. The impedance input of the absorber can be expressed by Eq. (6) [43].

$$R(\text{dB}) = 20 \lg \left| \frac{Z_{\text{in}} - 1}{Z_{\text{in}} + 1} \right| \tag{5}$$

$$Z_{\text{in}} = \sqrt{\frac{\mu_r}{\epsilon_r}} \tanh i \frac{2\pi f}{c} \sqrt{\mu_r \epsilon_r} d \tag{6}$$

where c represents the speed of light in free space, f is the frequency, and d is the thickness of the absorber.

Figure 5a–h show the three-dimensional reflection loss mapping plots of the four MWCNTs irradiated by microwaves at a thickness ranging from 0.1 mm to 5 mm. MI0-CNTs that has not been exposed to microwave irradiation exhibit moderate microwave absorption characteristics at 2–18 GHz, and its minimum reflection loss is at 4.6 GHz is -34.38 dB. After microwave irradiation with different durations, the minimum reflection loss of MI2-CNTs, MI4-CNTs and MI8-CNTs are -23.22 dB at 18 GHz, -34.95 dB at 5.4 GHz, and -45.74 dB at 13.8 GHz, respectively. It is worth noting that Fig. 5i–p provide calculation of the reflection loss curve and bandwidth of MI0-CNTs, MI2-CNTs, MI4-CNTs and MI8-CNTs, where the effective bandwidth is when the reflection loss is below -10 dB. The corresponding bandwidth, at which point the absorption efficiency of MWCNTs is 90%. Figure 5i, m show that the effective absorption bandwidth of MI0-CNTs is 3.9 GHz and the thickness ranges from 1.6 to 2 mm. In contrast, the effective absorption bandwidth of MI2-CNTs, MI4-CNTs and MI8-CNTs are concentrated at 10.8–16.7 GHz, 12.5–17.5 GHz and 12.5–17.5 GHz, and the absorber thicknesses are 2.6–3.5 mm, 1.6–2 mm and 1.6–2 mm. When the reflection loss is lower than -20 dB, that is, the absorption efficiency is 99%, the absorption bandwidth of MI4-CNTs and MI8-CNTs are concentrated at 14.9–17.2 GHz and 15.5–17.3 GHz when the absorption thickness is 1.6 mm. Based on the current requirements for thin thickness, light weight, strong absorption capacity and absorption bandwidth of microwave absorbers, the MI4-CNTs has the optimum reflection loss among the four samples, which showing that the microwave absorption performance of MWCNTs is enhanced as the degree of defects increases. Hence, combining with the defect intensity which has been revealed in previous characterizations, it can be seen that the defect density can be significant adjusted and further influenced the microwave absorption property. The corresponding performance modification could be attributed to the existence of different defect structures. These defect structures could destroy the structural symmetry at the atomic scale, leading to the separation of space charges and thus forming the electric dipoles. Under the external electromagnetic energy, these dipoles could oscillate and lead to dipolar polarization at the

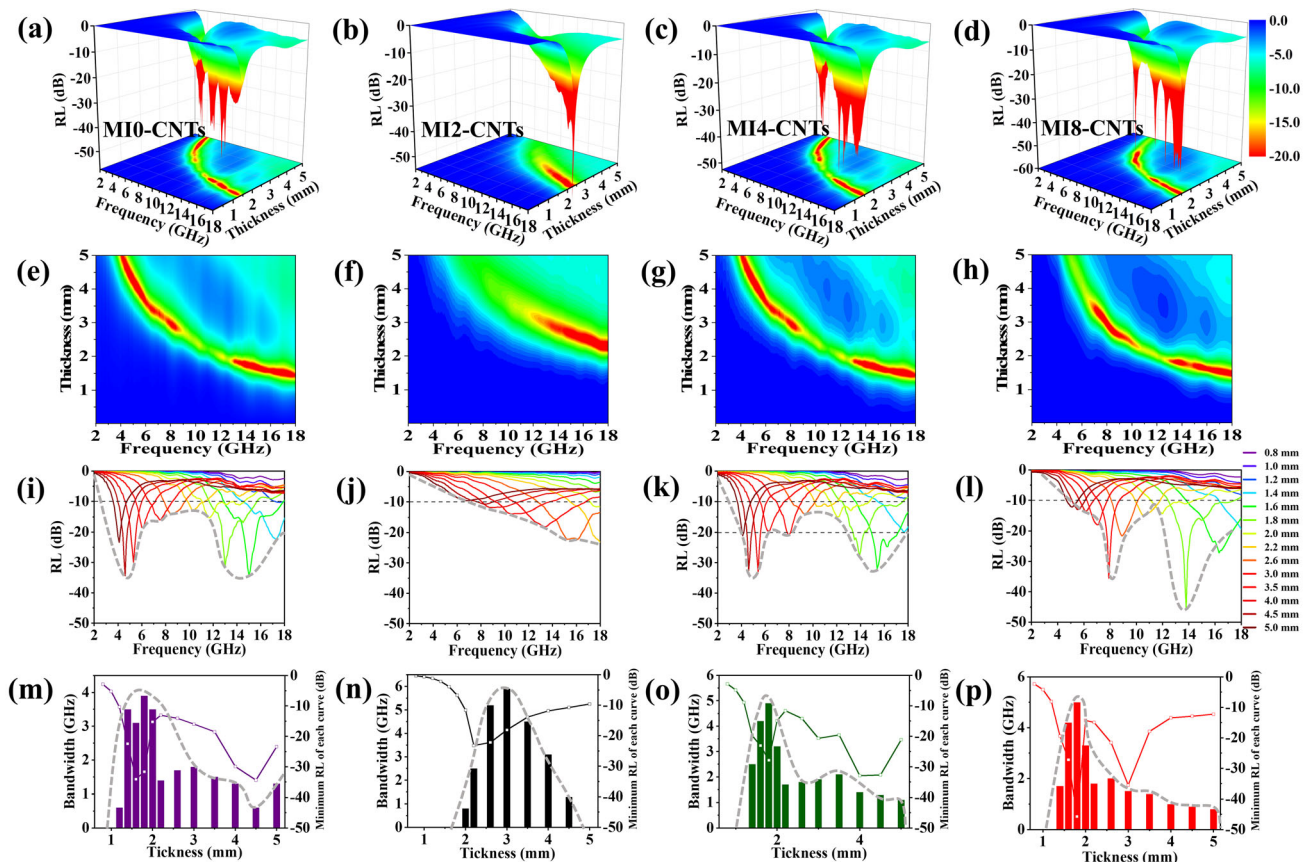


Figure 5 The three-dimensional reflection loss mapping, corresponding contour plots and microwave absorbing performances of MI0-CNTs, MI2-CNTs, MI4-CNTs and MI8-

defect sites, the polarization could thus improve the dielectric loss capacity and microwave absorption performance.

Conclusion

In this work, the microwave absorption characteristics of MWCNTs improved by microwave irradiation were studied. We found that the defect concentration changes with the microwave irradiation time, which leads to a series of changes in microwave absorption performance. In particular, there has been evidence that proper microwave radiation increases the density of defects in MWCNTs, and defects become centers of polarization, resulting in an increase in dielectric loss, thereby improving microwave absorption performance. The present study provides an efficient way to improve the microwave absorption properties by adjusting the density of defects

CNTs. **a–d** The three-dimensional reflection loss mapping; **e–h** the corresponding contour plots; **i–p** microwave absorbing performances.

through microwave irradiation instead of the conventional complicated process.

Acknowledgements

The authors gratefully acknowledge the National Natural Science Foundation of China (U1704253, 51471045), the Liaoning Revitalization Talents Program (XLYC1807177) and the fundamental research funds for the Central Universities (N160208001).

Compliance with ethical standards

Conflicts of interest The authors declare that they have no conflict of interest.

Electronic supplementary material: The online version of this article (<https://doi.org/10.1007/s10853-020-04996-7>) contains supplementary material, which is available to authorized users.

References

- [1] Wen B, Cao MS, Hou ZL, Song WL, Zhang L, Lu MM, Hai HB, Fang XY, Wang WZ, Yuan J (2013) Temperature dependent microwave attenuation behavior for carbon-nanotube/silica composites. *Carbon* 65:124–139
- [2] Kong L, Yin X, Yuan X, Zhang Y, Liu X, Cheng L, Zhang L (2014) Electromagnetic wave absorption properties of graphene modified with carbon nanotube/poly (dimethyl siloxane) composites. *Carbon* 73:185–193
- [3] Sun H, Che R, You X, Jiang Y, Yang Z, Deng J, Qiu LB, Peng HS (2015) Cross-stacking aligned carbon-nanotube films to tune microwave absorption frequencies and increase absorption intensities. *Adv Mater* 26:8120–8125
- [4] Wen F, Zhang F, Liu Z (2011) Investigation on microwave absorption properties for multiwalled carbon nanotubes/Fe/Co/Ni nanopowders as lightweight absorbers. *J Phys Chem C* 115:14025–14030
- [5] Lin S, Ju S, Shi G, Zhang J, He Y, Jiang D (2019) Ultrathin nitrogen-doping graphene films for flexible and stretchable EMI shielding materials. *J Mater Sci* 54:7165–7179. <https://doi.org/10.1007/s10853-019-03372-4>
- [6] Dang B, Chen Y, Wang H, Chen B, Jin C, Sun Q (2018) Preparation of high mechanical performance nano-Fe₃O₄/wood fiber binderless composite boards for electromagnetic absorption via a facile and green method. *Nanomaterials* 8:52
- [7] Iijima S (1991) Helical microtubules of graphitic carbon. *Nature* 354:56–58
- [8] Micheli D, Apollo C, Pastore R, Marchetti M (2010) X-Band microwave characterization of carbon-based nanocomposite material, absorption capability comparison and RAS design simulation. *Compos Sci Technol* 70:400–409
- [9] Li N, Huang Y, Du F, He XB, Lin X, Gao HJ, Ma YF, Li FF, Chen YS, Eklund PC (2006) Electromagnetic interference (EMI) shielding of single-walled carbon nanotube epoxy composites. *Nano Lett* 6:1141–1145
- [10] Cao MS, Yang J, Song WL, Zhang DQ, Wen BH, Jin B, Hou ZL, Yuan J (2012) Ferroferric oxide/multiwalled carbon nanotube vs polyaniline/ferroferric oxide/multiwalled carbon nanotube multiheterostructures for highly effective microwave absorption. *J ACS Appl Mater Inter* 4:6949–6956
- [11] Song WL, Guan XT, Fan LZ, Zhao YB, Cao WQ, Wang CY, Cao MS (2016) Strong and thermostable polymeric graphene/silica textile for lightweight practical microwave absorption composites. *Carbon* 100:109–117
- [12] Qing YC, Min DD, Zhou YY, Luo F, Zhou WC (2015) Graphene nanosheet- and flake carbonyl iron particle-filled epoxy-silicone composites as thin-thickness and wide-bandwidth microwave absorber. *Carbon* 86:98–107
- [13] Qing Y, Wang X, Zhou Y, Huang Z, Luo F, Zhou W (2014) Enhanced microwave absorption of multi-walled carbon nanotubes/epoxy composites incorporated with ceramic particles. *Compos Sci Technol* 102:161–168
- [14] Zhang KC, Gao XB, Zhang Q, Chen H, Chen XF (2018) Fe₃O₄ nanoparticles decorated MWCNTs @ C ferrite nanocomposites and their enhanced microwave absorption properties. *J Magn Magn Mater* 452:55–63
- [15] Qing Y, Nan H, Jia H, Min D, Zhou W, Luo F (2019) Aligned Fe microfiber reinforced epoxy composites with tunable electromagnetic properties and improved microwave absorption. *J Mater Sci* 54:4671–4679. <https://doi.org/10.1007/s10853-018-03192-y>
- [16] Vinayasree S, Soloman MA, Sunny V, Mohanan P, Kurian P, Joy PA, Anantharaman MR (2014) Flexible microwave absorbers based on barium hexaferrite, carbon black, and nitrile rubber for 2–12 GHz applications. *J Appl Phys* 116:024902
- [17] Yang WY, Zhang YF, Qiao GY, Lai YF, Liu SQ, Wang CS, Han JZ, Du HL, Zhang Y, Yang YC, Hou YL, Yang JB (2018) Tunable magnetic and microwave absorption properties of Sm_{1.5}Y_{0.5}Fe_{17-x}Si_x and their composites. *Acta Mater* 145:331–336
- [18] Watts PCP, Hsu WK, Barnes A, Chambers B (2010) High permittivity from defective multiwalled carbon nanotubes in the X-Band. *Adv Mater* 15:600–603
- [19] Li Y, Chen CX, Pan XY, Ni YW, Zhang S, Huang J, Chen D, Zhang YF (2009) Multiband microwave absorption films based on defective multiwalled carbon nanotubes added carbonyl iron/acrylic resi. *Phys B* 404:1343–1346
- [20] Wei HJ, Yin XW, Li X, Li MH, Dang XL, Zhang LT, Cheng LF (2019) Controllable synthesis of defective carbon nanotubes/Sc₂Si₂O₇ ceramic with adjustable dielectric properties for broadband high-performance microwave absorption. *Carbon* 147:276–283
- [21] Wu Y, Shu RW, Zhang JB, Sun RR, Chen YN, Yuan J (2019) Oxygen vacancy defects enhanced electromagnetic wave absorption properties of 3D net-like multi-walled carbon nanotubes/cerium oxide nanocomposites. *J Alloys Compd* 785:616–626
- [22] Stankovich S, Dikin DA, Piner RD, Kohlhaas KA, Kleinhammes A, Jia YY, Wu Y, Nguyen ST, Ruoff RS (2007) Synthesis of graphene-based nanosheets via chemical reduction of exfoliated graphite oxide. *Carbon* 45:1558–1565
- [23] Dresselhaus MS, Jorio A, Hofmann M, Dresselhaus G, Saito R (2010) Perspectives on carbon nanotubes and graphene raman spectroscopy. *Nano Lett* 10:751–758
- [24] Hasin P, Alpuche-Aviles MA, Wu Y (2010) Electrocatalytic activity of graphene multilayers toward I/I₃: effect of

- preparation conditions and polyelectrolyte modification. *J Phys Chem C* 114:15857–15861
- [25] Luo Y, Peng V, Qin FX, Adohi BJP (2014) Magnetic field and mechanical stress tunable microwave properties of composites containing Fe-based microwires. *Appl Phys Lett* 104:121912
- [26] Ferrari AC, Meyer JC, Scardaci V, Casiraghi C, Lazzeri M, Mauri F, Piscanec S, Jiang D, Novoselov KS, Roth S, Geim AK (2006) Raman spectrum of graphene and graphene layers. *Phys Rev Lett* 97:187401
- [27] Dresselhaus MS, Dresselhaus G, Saito R, Jorio A (2005) Raman spectroscopy of carbon nanotubes. *Phys Rep* 409:47–99
- [28] Cancado LG, Jorio A, Ferreira EHM, Stavale V, Achete CA, Capaz RB, Moutinho MVO, Lombardo A, Kulmala TS, Ferrari AC (2011) Quantifying defects in graphene via Raman spectroscopy at different excitation energies. *Nano Lett* 11:3190–3196
- [29] Guan GQ, Lu JS, Jiang HL (2016) Preparation, characterization, and physical properties of graphene nanosheets and films obtained from low-temperature expandable graphite. *J Mater Sci* 51:926–936. <https://doi.org/10.1007/s10853-015-9422-1>
- [30] Lin J, Peng ZW, Liu YY, Zepeda FR, Ye RQ, Samuel ELG, Yacamán MJ, Yakobson BI, Tour JM (2014) Laser-induced porous graphene films from commercial polymers. *Nat Commun* 5:5714
- [31] Cancado LG, Takai K, Enoki T, Endo M, Kim YA, Mizusaki H, Jorio A, Coelho LN, Magalhães-Paniago R, Pimenta MA (2006) General equation for the determination of the crystallite size L_a of nanographite by Raman spectroscopy. *Appl Phys Lett* 88:163106
- [32] Zafar Z, Ni V, Wu V, Shi ZX, Nan HY, Bai J, Sun LT (2013) Evolution of Raman spectra in nitrogen doped graphene. *Carbon* 61:57–62
- [33] Eigler S, Dotzer C, Hirsch A (2012) Visualization of defect densities in reduced graphene oxide. *Carbon* 50:3666–3673
- [34] Cao AY, Xu CL, Liang J, Wu DH, Wei BQ (2001) X-ray diffraction characterization on the alignment degree of carbon nanotubes. *Chem Phys Lett* 344:13–17
- [35] Rupak K, Kumar GA (2015) APTES grafted ordered mesoporous silica KIT-6 for CO₂ adsorption. *Chem Eng J* 262:882–890
- [36] Lv HF, Mu SC (2014) Nano-ceramic support materials for low temperature fuel cell catalysts. *Nanoscale* 6:5063
- [37] Baghbanzadeh M, Carbone L, Cozzoli PD, Kappe CO (2011) Microwave-assisted synthesis of colloidal inorganic nanocrystals. *Angew Chem Int Ed* 50:11312–11359
- [38] Rafaja D, Schimpf C, Klemm V, Schreiber G, Bakonyi I, Péter L (2009) Formation of microstructural defects in electrodeposited Co/Cu multilayers. *Acta Mater* 57:3211–3222
- [39] Ji JY, Sui G, Yu YH, Liu YX (2015) Significant improvement of mechanical properties observed in highly aligned carbon-nanotube-reinforced nanofibers. *J Phys Chem C* 113:4779–4785
- [40] Watts PCP, Hsu WK, Harold WK, David RMW (2003) Are bulk defective carbon nanotubes less electrically conducting. *Nano Lett* 3:549–553
- [41] Hammond P (2013) *Applied electromagnetism*. Elsevier, Amsterdam
- [42] Qin FX, Peng HX, Fuller J, Brosseau C (2012) Magnetic field-dependent effective microwave properties of micro-wire-epoxy composites. *Appl Phys Lett* 101:323
- [43] Wang ZH, Wang JY, Li YX, Liu RG, Zhang YH, Zhao XN, Zhang XF (2018) Multi-interfacial Co@CoNx@C(N) nanocapsules with nitrogen substitutions in graphitic shells for improving microwave absorption properties. *J Alloys Compd* 736:51–56

Publisher's Note Springer Nature remains neutral with regard to jurisdictional claims in published maps and institutional affiliations.